*J Mater Sci* (2017) 52:2628–2641

# The effect of liquid crystal fillers on structure and properties of liquid crystalline shape memory polyurethane composites II: 4-hexadecyloxybenzoic acid

Jianfeng Ban[1,2], Linjiang Zhu[1], Shaojun Chen[1,*], and Yiping Wang[2,*]

[1] *Guangdong Research Center for Interfacial Engineering of Functional Materials, Shenzhen Key Laboratory of Polymer Science and Technology, Nanshan District Key Lab for Biopolymers and Safety Evaluation, College of Materials Science and Engineering, Shenzhen University, Shenzhen 518060, China*

[2] *Key Laboratory of Optoelectronic Devices and Systems of Ministry of Education and Guangdong Province, College of Optoelectronic Engineering, Shenzhen University, Shenzhen 518060, China*

**Received:** 8 August 2016
**Accepted:** 31 October 2016
**Published online:** 9 November 2016



## ABSTRACT

In order to better understand the interrelation between liquid crystal fillers and functional polymers, a series of liquid crystalline shape memory polyurethane composites (LC-SMPUCs), named shape memory polyurethane (SMPU)–4-hexadecyloxybenzoic acid (HOBA) composites, are prepared by incorporating HOBA into SMPU based on a polyethylene glycol (PEG) soft segment. The results demonstrate that the dimerization structure of HOBA is maintained in the as-prepared SMPU–HOBA composites, facilitating liquid crystalline properties. Characterization results display smectic C phase upon heating, while the isotropic temperature shifts to a higher temperature, broadening the temperature range of the liquid crystalline phase. The SMPU–HOBA composites form a two-phase separated structure containing a SMPU phase and a HOBA phase; the incorporated HOBA can promote crystallizability of both soft and hard segments of SMPU, while crystalline hard phases are maintained within the high temperature range. Thus, SMPU–HOBA composites demonstrate a two-step modulus change upon heating that releases a triple-shape memory effect. The final shape fixing ratio is higher than 99%, and the final shape recovery ratio reaches 90%. Therefore, the SMPU–HOBA composites successfully provide a desirable combination of liquid crystalline properties and triple-shape memory properties, making them ideal candidates for smart sensor, smart labels, etc.

Address correspondence to E-mail: chensj@szu.edu.cn; ypwang@szu.edu.cn



DOI 10.1007/s10853-016-0554-8

## Introduction

As an important stimulus-responsive material, shape memory polymers (SMPs) have been widely studied due to their capability of recovering their original shapes upon exposure to external stimuli. [1–4] The bulk of the research to date has been concentrated on thermal-induced SMPs with a wide range of activation temperatures and applications, such as use in medical devices and surgical materials, heat-shrinkable packages for electronics, mechanical actuators, temperatures sensors, and self-deployable structures. [2–6] Among thermal-induced SMPs, shape memory polyurethane (SMPU) has been most commonly utilized in practice due to its competitive mechanical and shape memory properties [7–11]. However, the common SMPU displaying only a shape memory effect (SME) has not been able to meet the growing trend of new multi-functional materials. Shape memory polymer composites (SMPCs) functionalized with different fillers have significantly broadened the varieties and functionalities of SMPs [12–16]. The developed new functionalities make SMPCs increasingly useful in both scientific endeavors as well as industrial applications. Taking into consideration the various kinds of functional fillers, liquid crystals (LC) have recently attracted much attention due to their wide use in the fabrication of various advanced functional materials [17–19]. Finkelmann et al. [20] first reported a liquid crystalline elastomer with photo-illuminated SMEs by incorporating azo-containing LCs in the polymer elastomer. Sonin et al. [21] also prepared a liquid crystalline polymer composite for optical irradiation control. Additionally, Ahir et al. [22] synthesized a novel tri-block copolymer with significant two-way SME. These studies motivate this investigation to further develop similar smart materials with LC fillers to elucidate liquid crystalline properties in the resultant composite.

Recently, we successfully developed a facile and versatile method to prepare SMPCs by incorporating LC fillers to SMPs. The obtained LC-based SMPCs (named LC-SMPCs) not only maintained the liquid crystalline properties of the LC fillers, but also behaved with new functional abilities, such as triple-SME, quadruple-SME, and self-healing properties [23, 24]. In order to select a suitable polymer matrix for LC-SMPCs, after selecting 4-hexadecyloxybenzoic acid (HOBA) as the constant LC filler, a variety of SMPUs based on different reversible phases, such as amorphous soft phase, semi-crystalline soft phase, and supramolecular switches, were systematically studied in literature. In the amorphous SMPU–HOBA composites, the glass transition temperature ($T_g$) of the amorphous soft phase shifts to a lower temperature, while the HOBA maintains its intrinsic crystalline and liquid crystalline properties. Both the glass transition of SMPU and crystal melting transition of HOBA could be implemented to trigger triple-SME [24]. In the semi-crystalline SMPU–HOBA composites, both crystallization temperature ($T_c$) and its crystal melting temperature ($T_m$) of the soft phase shift to a higher temperature, while the doped HOBA fillers are divided into two parts: crystal-dispersed HOBA and free HOBA [23]. Thus, the material displays not only triple-SME, but also thermal-induced self-healing properties. Additionally, in the supramolecular liquid crystalline SMPU complex, hydrogen-bonded HOBA phase is formed via hydrogen bonding between pyridine rings and the –COOH group of HOBA. The supramolecular LC-SMPCs also displayed suitable triple-SMEs and liquid crystalline properties [25]. Recent insights into LC-SMPC filled with 4-*n*-octyldecyloxybenzoic acid (OOBA) further demonstrate that SMPU–OOBA composites can also display adequate multi-SMEs, exhibiting triple-SMEs and quadruple-SMEs [26]. These studies provide an exhaustive understanding about the influence of the SMP matrix on the LC-SMPCs. SMPU maintains its micro-phase separation structure for exhibiting SMEs, while HOBA filler maintains its original dimerization structure for exhibiting liquid crystalline properties. However, to date, the influence of LC fillers on the LC-SMPUs has not been well reported in which the interrelation between LC fillers and SMPU remains unclear.

Aiming to further understand the interrelations between LC fillers with the polymer matrix of LC-SMPCs and promoting their future applications, the effect of LC fillers on the structure, morphology, and properties of LC-SMPCs has been systematically investigated. By selecting a control SMPU based on a PEG semi-crystalline soft segment and 40 wt% MDI-BDO hard segments, a series of LC-SMPCs of various LC fillers, such as HOBA, OOBA, and DOBA, were prepared. The LC fillers were selected due to pure OOBA and HOBA reportedly showing only nematic and smectic phases, respectively, while pure DOBA displays both nematic and smectic phases. The

impact of OOBA and DOBA on LC-SMPCs will be reported in another paper [27]. Being notably different from previous systems, the present LC-SMPCs were prepared by incorporation of HOBA to the PEG-based SMPU. This study lays the foundation for the impact of HOBA filler on the structure, morphology, and multi-functional properties of SMPU–HOBA composites.

## Experimental section

### Materials

HOBA (analytical grade) was purchased from the Jiaxing Carry Bio-Chem Technology Co. Ltd. (Zhejiang, China). Polyethylene glycol (PEG, $M_n = 6000$ g/mol), Diphenylmethane diisocyanate (MDI, analytical grade), 1,4-butanediol (BDO, analytical grade), and dimethylformamide (DMF, high-performance liquid chromatography grade, solvent) were purchased from Aladdin Chemical Reagent Co. Ltd. (Shanghai, China). PEG was dried beforehand at 80 °C under 0.1–0.2 MPa for 6 h.

### Preparation of SMPU–mHOBA composites

As stated in our previous work [28], the PEG-based SMPU with 40 wt% hard segment content (SMPU40) was synthesized via bulk polymerization method with MDI, BDO, and PEG. Firstly, a 10 wt% SMPU/DMF solution was prepared by dissolving the obtained bulk SMPU40 into DMF at 80 °C for 48 h. Based on the composition shown in Table 1, a certain quantity of HOBA, e.g., 1.68 g, was added to the SMPU/DMF solution containing approximately 3.0 g SMPU resin. Under strong mechanical stirring at 80 °C for 2 h, the SMPU and the HOBA were mixed to obtain a homogeneous solution-phase mixture. Finally, solvent-cast films for the following tests were obtained by casting the solution mixture onto a Teflon pan, which was dried at 80 °C for 24 h and further dried at 80 °C under a vacuum for 24 h. The samples were labeled as SMPU–mHOBA (coded as P1–P5), in which m is the molar ratio of C=O/N–H, e.g., sample SMPU–HOBA0.2, coded as P1.

### Instruments and measurements

Fourier transform infrared spectra (FT-IR) were scanned from smooth polymer films with a thickness of 0.2 mm using a Nicolet 6700 FT-IR spectrometer (Nicolet, USA) by the FT-IR-attenuated total reflection (ATR) method. Liquid $N_2$-cooled mercury cadmium telluride (MCT) was used as a detector, and ZnSe crystals are used for ATR. Ten scans at 4 $cm^{-1}$ resolution were averaged and stored as data files for further analysis.

The surface morphology of the samples was examined using scanning electron microscopy (SEM, SU-70, Hitachi, Japan), 20 kV, equipped with an energy dispersive X-ray detector for elemental composition. Prior to scanning, the samples were coated with a thin layer of gold. Fraction morphology was scanned after the samples were fractured with liquid nitrogen.

Thermo Gravimetric Analyzer (TGA) spectra were recorded on a computer-controlled TG Q50 system (TA, USA) after drying at 100 °C, under the following operational conditions: heating rate 10 °C/min, temperature range 100–600 °C, sample weighed about 5.0 mg, using the film sample in platinum crucibles, 60 mL/min $N_2$ flow.

Differential scanning calorimetry (DSC) measurements were carried out via a TA Q200 instrument (TA, USA) by utilizing nitrogen as the purged gas. Indium and zinc standards were used for calibration. Both heating scan rate and cooling rate are 10 °C/

**Table 1** Composition of SMPU–mHOBA composites

| Samples | SMPU40 (g) | HOBA (g) | $R^a$ | HOBA content (wt%) |
|---|---|---|---|---|
| Pure SMPU | 3.0 | 0 | 0 | 0.0 |
| P1(SMPU–0.2HOBA) | 3.0 | 0.24 | 0.2 | 7.3 |
| P2(SMPU–0.4HOBA) | 3.0 | 0.47 | 0.4 | 13.6 |
| P3(SMPU–0.6HOBA) | 3.0 | 0.71 | 0.6 | 19.1 |
| P4(SMPU–0.8HOBA) | 3.0 | 0.94 | 0.8 | 23.9 |
| P5(SMPU–1.0HOBA) | 3.0 | 1.18 | 1.0 | 28.2 |

[a] $R$: Molar ratio of C=O/N–H

min. The second heating curves were used for analysis.

Dynamic mechanical analysis (DMA) curves were determined using a DMA Q800 system (TA, USA) at 1 Hz, and at a heating rate of 2 °C/min. Rectangle specimen with a thickness of 0.5 mm was used.

A Nanonavi E-Sweep (SII Nanotechnology Inc.) atomic force microscope (AFM) was used in tapping mode for the morphological characterization of the dried sample. The samples were dissolved in DMF at a concentration of 5 mg/mL and firstly spin-coated at 400 rpm for 10 s followed by 4000 rpm for 60 s on oxidized silicon substrates. Spin-coated films were kept in a 50 °C oven for 48 h to evaporate the solvent. *Meso*-phases were identified and the phase transition temperatures were determined using a POM microscope (Mshot, China) equipped with a hot stage (Metter Toledo FP90 central processor) at a scan rate of 2 °C/min. The samples were heated from 25 to 160 °C and cooled from 160 to 25 °C.

Thermally induced triple-shape memory behaviors were examined via thermomechanical analysis using the DMA Q800 system (TA, USA) with tension clamps in controlled force mode according to the procedure described in previous publications. Samples were dried at 100 °C for 24 h and cut into rectangular specimens of 10 mm × 2.0 mm × 0.5 mm dimensions.

## Results and discussion

### Structural analysis

It is conventionally known that carboxylic acid groups form strong intermolecular hydrogen bonding. HOBA displays liquid crystalline properties due to its dimerization structure through hydrogen bonding, creating a long lath-like structure with a three-ring core (see supporting information Fig. S1) [29, 30]. In this experiment, structural analysis of SMPU–mHOBA composites is performed on the basis of carbonyl acid groups of HOBA. Figure 1 shows the FT-IR spectra of HOBA, pure SMPU, and sample P5. The O–H stretching vibration is detected at approximately 3445 $cm^{-1}$ in the spectrum of HOBA. The N–H stretching vibration at approximately 3323 $cm^{-1}$ exhibits the formation of urethane groups (–NHCOO–) and is observed in the spectra of the pure SMPU and P5. On comparing with the pure

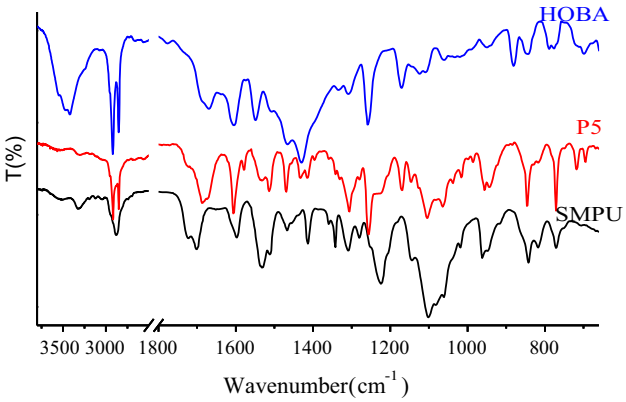


**Figure 1** FT-IR spectra of HOBA, the pure SMPU, and sample P5.

SMPU, the SMPU–mHOBA composite, e.g. P5, shows new frequencies at approximately 1260, 1163, and 1050 $cm^{-1}$; these frequencies are also detected in the spectrum of HOBA. It is thus confirmed that the HOBA is successfully incorporated into the SMPU to form a SMPU–mHOBA composite. However, no significant differences were observed in the N–H vibration frequency at approximately 3396 $cm^{-1}$ or the C=O vibration frequency at 1669 $cm^{-1}$ in all SMPU–mHOBA composites at varying HOBA contents (see supporting information Fig. S2). This result implies that the doped HOBA does not influence the original hydrogen bonding between the N–H group and the C=O group of the urethane groups. In previous work, the liquid crystalline phase appeared to disappear when LC mesogens containing pyridine moieties were attached to the SMPU-containing carboxyl groups through hydrogen bonding between pyridine and COOH [31]. However, the SMPU–mHOBA composite is a simple physical mixture of HOBA with SMPU in this work. HOBA tends to keep its intrinsic liquid crystalline properties in the composites.

### Morphology analysis

Similar to the previous LC-SMPU composites [23, 24], the present SMPU–mHOBA composites not only maintain their liquid crystalline properties of their respective fillers, but also can be implemented as polymeric materials for a variety of applications. However, the disadvantage of LC incorporation is that high content of LC fillers might destroy the surface morphology of SMPU. The surface morphology of the SMPU–mHOBA composites is

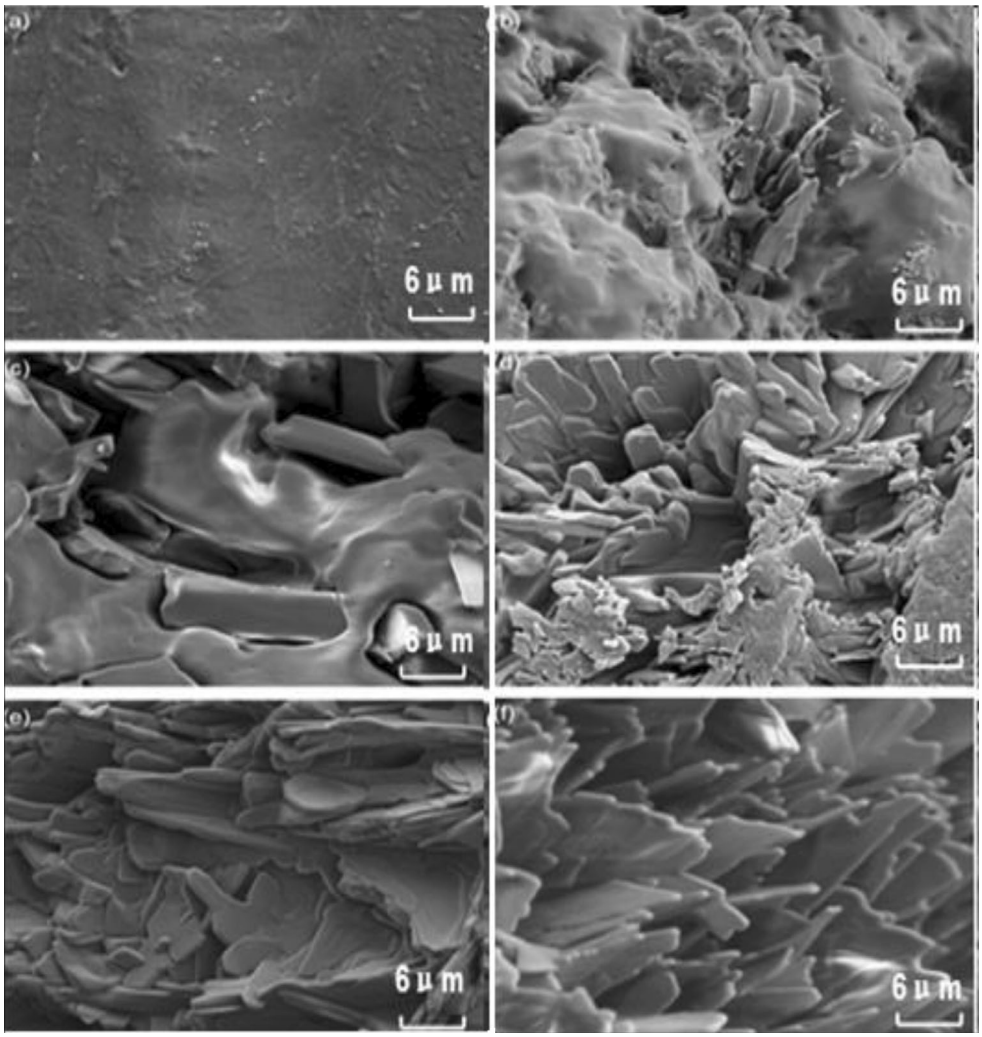


**Figure 2** SEM images of samples (**a** the pure SMPU, **b** sample P1, **c** sample P2, **d** sample P3, **e** sample P4, and **f** the pure HOBA).

systematically investigated in this study. Figure 2 displays the SEM images of polymeric films prepared from SMPU–mHOBA composites with various HOBA content. As shown in Fig. 2a, the pure SMPU has a smooth surface without any holes, whereas the surface of the composites becomes rough when the HOBA is doped into the SMPU. As the HOBA content increases, an increasing number of cracks are observed in the samples P2, P3, P4, and P5 (see Fig. 2b–e). When compared with the SMPU–mOOBA and SMPU–mDOBA composites (see supporting information Fig. S3, S4), to form continuous complete polymeric films, the doped HOBA content should not exceed a content of approximately 24 wt% in the SMPU–0.8HOBA composites, while only 18 wt% OOBA or 21 wt% DOBA is capable of being doped in the SMPU–0.8OOBA and SMPU–0.8DOBA composites, respectively. Results suggest that the doped LC content increases as the length of tail chain increases. The higher LC content tends to display improved liquid crystalline properties in the LC-SMPU composites. Additionally, the longer tail chain appears to promote crystallization within the composite. A moderate quantity of completed HOBA crystals is clearly observed in the SEM images of SMPU–mHOBA composites (see Fig. 2e, f). Thus, the SEM images demonstrate a two-phase separated structure composed of the crystalline HOBA phase and the amorphous SMPU matrix in all SMPU–mHOBA composites (see Fig. 2c, d). Furthermore, it is confirmed that the doped HOBA is either surrounded by the polyurethane matrix or self-assembled into the free HOBA phase. AFM images further confirm the micro-phase separated structure of the SMPU matrix. The height and phase images of P4 show that light and shaded cross-distribution micro-areas exist in the

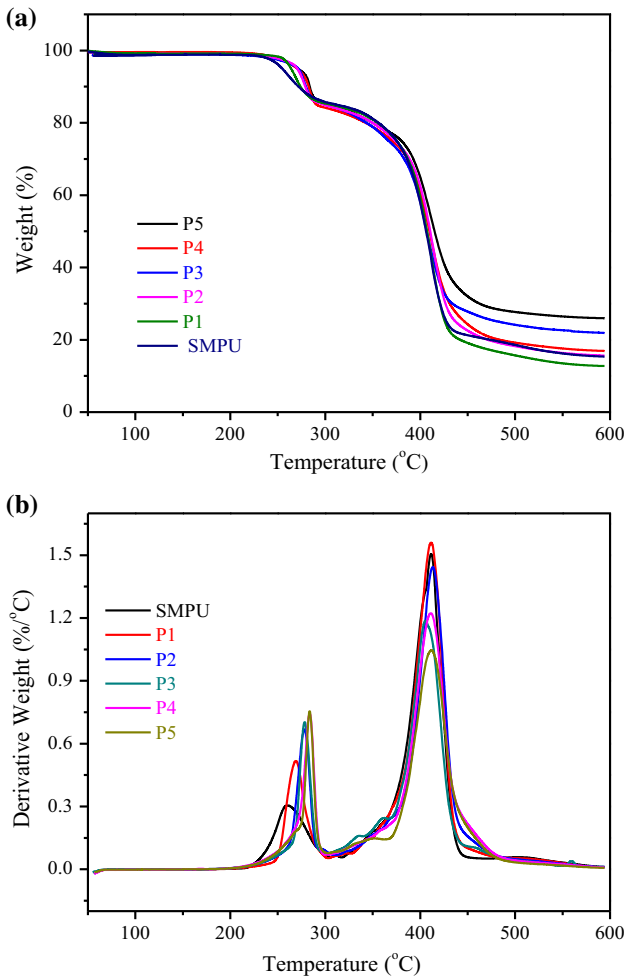


**Figure 3** TG–DTG curves of the samples, **a** TG curves, **b** DTG curves.

polyurethane matrix. Outshoots appear throughout the surface that corresponds to the lightly colored parts in the AFM images, representing the hard phase of polyurethane. The concave parts (describing continuous phases) could represent the soft phase, as explained in supporting information (see Fig. S5). In conjunction with SEM results, the continuous repeating peak in AFM indicates that the polyurethane matrix maintains suitable micro-phase separation structure of SMPU, providing a morphology foundation for exhibiting shape memory properties.

## Thermal properties

Thermal property of composite is a critical property for applications of LC-SMPCs as polymeric materials. The thermal properties of the SMPU–mHOBA composites were investigated via TGA and DSC measurements. The TG curves of the SMPU–mHOBA verify that all samples decompose in two stages, corresponding to the decomposition of the urethane moiety (200–300 °C) and the soft segments (350–450 °C) of the SMPU (see Fig. 3a). This decomposition behavior appears to be identical to pure SMPU and the previous LC-SMPCs. This result suggests that the thermal stability of the polymer matrix is also maintained in the SMPU–mHOBA composites. Additionally, TG results further verify that the decomposition temperature of the SMPU–mOOBA composites increases as HOBA content increases, thus implying that the incorporated HOBA assists in improving the thermal stability of SMPU. Furthermore, the DTG curves reveal that the maximum decomposition temperatures of the first stage in the composites were higher than pure SMPU (see Fig. 3b). One explanation for this difference may be that the decomposition degree of the SMPU–mHOBA composites is restrained when HOBA is doped into the SMPU. Hence, it is confirmed that the improved thermal stability yields ideal polymeric-based composites.

Significant influence of HOBA fillers on the thermal properties is reflected by the DSC curves. Figure 4a presents a comparison of thermal properties of the pure SMPU, HOBA, and sample P2. The second heating DSC curve of the pure SMPU shows an exothermic peak at −5 °C and an distinct endothermic peak at 49.5 °C (see Fig. 4a), corresponding to the heat-induced $T_c$ and $T_m$ of the soft phase of SMPU, respectively. As previously described in literature [25], the pure HOBA has a heat-induced $T_c$ at 65 °C, and typically exhibits two types of crystals with a $T_m$ appearing at approximately 19 and 101 °C. The weak endothermic peak at 123 °C demonstrates the phase transition from the liquid crystalline phase to the isotropic phase, namely the isotropic temperature ($T_i$). When HOBA is physically mixed with the PEG-based SMPU to form LC-SMPU composites, e.g., sample P2, the $T_m$ of polyurethane shifts to a higher temperature and the cold crystallization observed in the pure SMPU and HOBA disappears. These results suggest that the crystallization capacity of the soft segment of SMPU is enhanced upon the introduction of HOBA to the composite, while the crystallization capacity of HOBA is hindered due to the interruption of its regularity by the SMPU polymer chains.

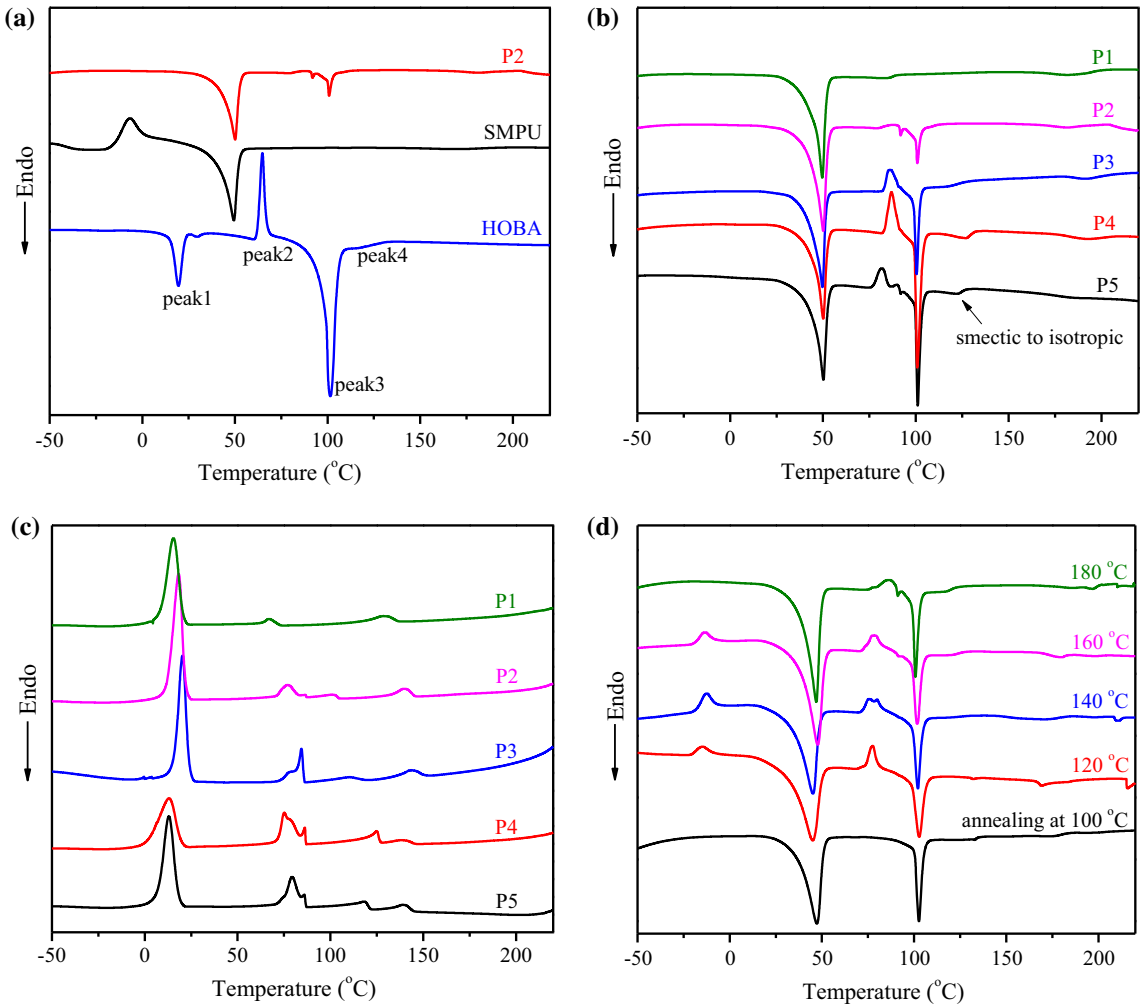


**Figure 4** Thermal properties of the composites **a** the second heating DSC curves of HOBA, pure SMPU, and P2, **b** the second heating DSC curves of SMPU–mHOBA composites, **c** the first cooling DSC curves of SMPU–mHOBA composites, and **d** the influence of annealing temperature on sample P2.

Figure 4b presents the effects of HOBA content on the various synthesized composites. As the HOBA content increases, the $T_m$ of the soft phase of SMPU shifts to a higher temperature. This result further confirms enhanced crystallization of the soft phase of SMPU due to the incorporated HOBA serving as crystal seeds. On comparing with pure SMPU, Fig. 4b also demonstrates that the $T_m$ of the hard phase of SMPU becomes apparent at ca. 183 °C in the composites and appears to shift to higher temperature as the HOBA content increases. A possible reason is that the HOBA crystals provide nucleation sites for the crystallization of the hard phase. Additionally, the cooling curves demonstrate that SMPU–mHOBA composite shows a series of endothermic peaks upon cooling (see Fig. 4c). Taking P5 as an example, the peak at 13.1 °C is attributed to the $T_c$ of the soft phase of SMPU and it is relatively higher compared to pure SMPU. Hence, it is once more confirmed that HOBA assists to promote the crystallization of the soft phase. The peak at 78.8 °C is attributed to the $T_c$ of the HOBA phase, and the endothermic peak at 118.9 °C shows the phase transition from the isotropic phase to the LC phase. However, the peak at 140.9 °C should be attributed to the $T_c$ of the hard phase of SMPU. These phase transitions are also verified by the following POM investigations.

To better understand the interaction between HOBA and the polyurethane chain, the influence of heat treatment is also investigated. Figure 4d demonstrates the second heating DSC curves of sample P2 after annealing at different heat-treated

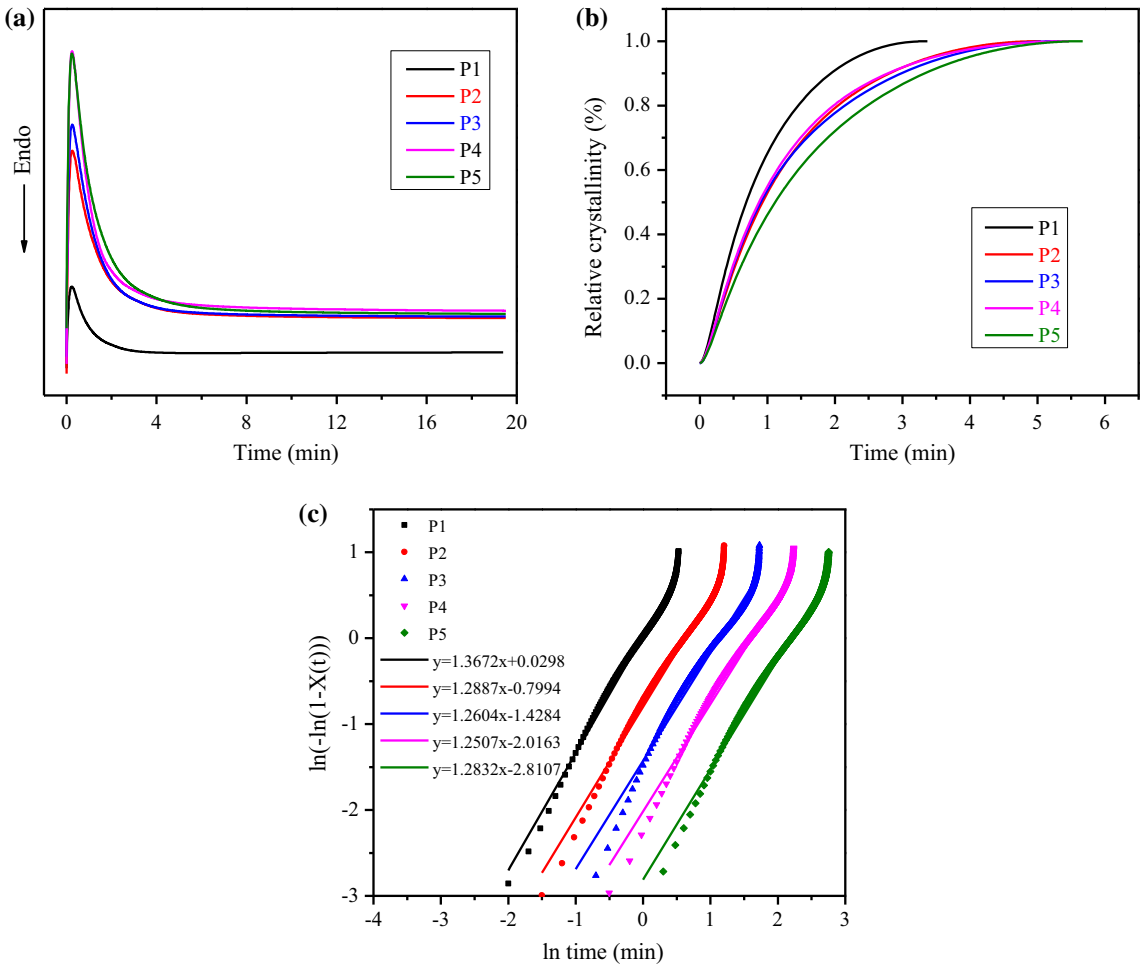


**Figure 5** Isothermal crystallization of the SMPU–mHOBA composites, **a** exothermic curves versus time, **b** dependency of relative crystallinity versus time, **c** plots of $\log\{-\ln[1 - X(t)]\}$ versus log$t$ and the fitting line at 137 °C.

temperatures. When sample P2 is thermally treated at 120, 140, and 160 °C, the cold crystallization peak of the soft phase of SMPU is detected at −13 °C. However, this cold crystallization peak disappears after thermal treatment at 100 and 180 °C. A possible hypothesis to explain this behavior is that the movement of the polymer chains is frozen at the low heat-treated temperatures (e.g., 100 °C), while the higher heat-treated temperatures (e.g., 180 °C) promote the movement of polymer chains and cause a complete crystallization of the soft segments upon cooling. In addition, Fig. 4d also demonstrates that the $T_m$ of both the soft and hard phases of SMPU shifts to a higher temperature as the thermal treatment temperature increases, which indicates that the increased heat-treated temperature promotes crystallization of the soft and hard segments of SMPU. Therefore, heat treatment provides a facile method to adjust the phase transitions of LC-SMPCs that might influence the liquid crystalline properties and shape memory properties.

To further understand the crystallization behaviors of the SMPU–mHOBA composites, the isothermal crystallization process was investigated. The isothermal crystallization kinetics was characterized according to the procedure described in previous publications [32]. The sample (4–6 mg) was initially heated to 230 °C at a rate of 10 °C/min and maintained for 5 min to remove the thermal history. Subsequently, the sample was cooled rapidly (−60 °C/min) to a designated $T_c = 137$ °C. The sample was then held at this temperature until the end of the exothermic crystallization. The heat flow was recorded as a function of time during the isothermal crystallization process. Figure 5a presents the isothermal crystallization exothermic peak of the

SMPU–mHOBA composites. As the HOBA content increases, the heat flow of composite significantly increases which confirms enhanced crystallization of the hard phase. According to the heat flow or the isothermal crystallization exothermic peak, a relative crystallinity ($X_t$) can be calculated. Figure 5b presents the relationship between $X_t$ and time ($t$). The S pattern implies that that the crystallization rate is relatively slow during the initial and latter stages of crystallization. Figure 5b also demonstrates that the slopes of the curves decrease with an increase in HOBA content, thus suggesting that the crystallization rate of the hard phase decreases as the HOBA content increases. Additionally, the complete crystallization behaviors of the SMPU–mHOBA composites could be also characterized with the *Avrami* equation. The *Avrami* equation can be further converted to another equation via linearization as follows [32]:

$$\ln[-\ln(1 - X_t)] = n \ln t + \ln K$$

The dependency of $\log\{-\ln[1 - X(t)]\}$ on $\log t$ could be obtained as shown in Fig. 5c. Even though the curve slightly deviates at the end of crystallization due to the phase transformation from spherocrystal to lamellar crystal, $\log\{-\ln[1 - X(t)]\}$ and $\log t$ display an adequate linear relation. According to the linear relation and line fit, the kinetic parameters $n$, $K$, and $t_{1/2}$ could be calculated (see Table 2). Similar to the previous SMPU–mDOBA composites and SMPU–mOOBA composites, the n values are also ~1.3 in the SMPU–mHOBA composites. Hence, this confirms that the crystallization mechanism of the hard segment of SMPU is the nucleated mechanism, and the HOBA provides nucleation sites (seeds) for the crystallization of the hard phase.

**Table 2** Isothermal crystallization kinetic parameters for SMPU–mHOBA composites

| Sample | $n$ | ln$K$ | $K$ | $t_{1/2}$ |
|---|---|---|---|---|
| P1 | 1.3 | 0.03 | 1.03 | 0.75 |
| P2 | 1.3 | −0.80 | 0.45 | 1.40 |
| P3 | 1.3 | −1.43 | 0.24 | 2.32 |
| P4 | 1.3 | −2.021 | 0.13 | 3.74 |
| P5 | 1.3 | −2.81 | 0.06 | 6.72 |

$K$ is the Avrami parameter, $n$ is the Avrami index, $t_{1/2}$ is the half-crystallization time

## Liquid crystalline properties

The phase transition behavior and liquid crystalline properties of SMPU–mHOBA composites were investigated via POM. To maintain consistency among DSC results, all samples were heated to the same high temperature used for the DSC tests and then slowly cooled to room temperature before POM measurements. According to our previous investigations, the pure SMPU exhibits only a crystalline texture below 40 °C (see Fig. S6). The pure HOBA maintains no phase transition below 81 °C, and it shows a transition to a smectic C phase at 106 °C, while the smectic–isotropic phase transition appears at 125 °C (see Fig. S7). This process is consistent with DSC measurements (see Fig. 5a). When the HOBA is incorporated into SMPU, the phase transition behaviors are affected in the SMPU–mHOBA composites. Figure 6 presents the POM pictures of samples P2 at different temperatures upon heating. P2 shows a bright abundant crystalline texture at 43 °C (see Fig. 6a) due to the overlapping crystallization of the soft phases of SMPU and HOBA. When the temperature is increased to 79 °C, thermal-induced crystallization is observed, suggesting the formation of a second type of crystals of HOBA (see Fig. 6b); this observation is consistent with DSC results of HOBA. Furthermore, at 113 °C, the POM image shows a clear two-phase separation structure. The isolated phase shows clear liquid crystalline texture, while the continuous dark phase is a result from the SMPU matrix (see Fig. 6c). When the temperature is higher than 113 °C, the liquid crystalline texture gradually disappears; the field of vision becomes dark, indicating the phase transition from a liquid crystalline state to the isotropic state. On comparing with the pure HOBA, the $T_i$ shifts to lower temperatures in all SMPU–mHOBA composites. A possible hypothesis is that the HOBA is restrained by the SMPU matrix. In addition, the POM images also demonstrate that another crystalline phase showing Maltese crosses pattern does not disappear until the temperature is higher than 167 °C (see Fig. 6d). This pattern results from the spherical crystals of MDI-BDO hard segment of SMPU, confirming the existence of a crystalline hard phase; this phenomenon is also confirmed by means of DSC measurements.

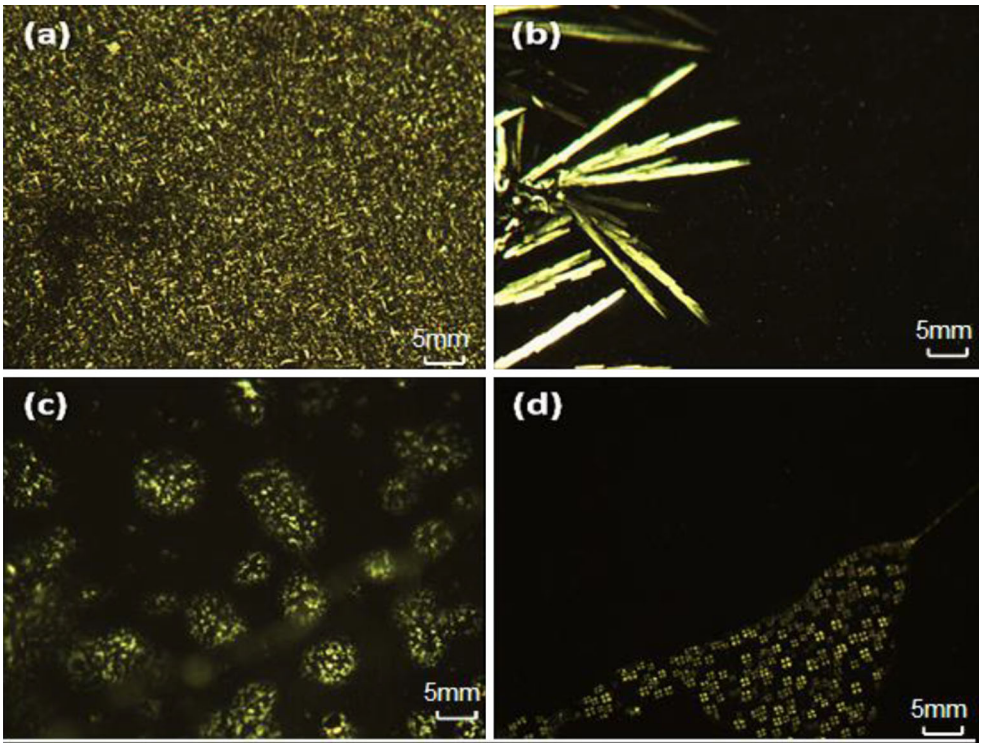


**Figure 6** POM images (×400) of sample P2 upon heating (**a** 44 °C, **b** 79 °C, **c** 113 °C, **d** 167 °C).

## Dynamical mechanical properties

DMA measurements can be implemented in order to investigate the phase transitions of the synthesized composites in this investigation. Figure 7 presents the DMA curves of the pure SMPU and SMPU–mHOBA composites with varying HOBA content. The DMA curves reveal that all samples demonstrate their largest storage modulus during the glassy state, whereas a significant decrease in storage modulus occurs at 48 °C due to the crystals melting of the soft phase of SMPU, as shown in Fig. 7a. On comparing with the pure SMPU, SMPU–mHOBA composites display two rubbery state modulus platforms. The second decrease in storage modulus is found within the temperature range of 100–120 °C, particularly with the composites containing higher HOBA content. This change can be attributed to the crystal melting transition of HOBA due to its relationship to $T_m$ of HOBA. Therefore, the HOBA phase provides a second reversible phase that facilitates a switch of storage modulus. The tan$\delta$ curves further demonstrate the pure SMPU exhibiting two peaks, a $T_g$ and a $T_m$ peak of the soft phase, whereas the composites display an additional transition peak at about 110 °C, as shown in Fig. 7b. As the HOBA content increases, the peak intensity of the $T_g$ transition becomes weaker while the peak intensity of $T_m$ of soft phase becomes stronger. A possible explanation for this is that the incorporated HOBA lubricates the polymer chains during the $T_g$ transition serving as a lubricant agent, while the HOBA crystals improve the storage loss during the $T_m$ transition by acting as crystallization seeds. According to the multi-phase structure requirement for triple-shape memory functionality, the SMPU–mHOBA composites exemplify multiple phase transitions with a significant multi-step modulus change, indicating said composites are expected to show a triple-shape memory effect.

## Shape memory properties

Firstly, the thermal-induced shape memory properties of SMPU–mHOBA composites were qualitatively investigated. A specimen with a rectangular pattern was prepared using the film of sample P3. The sequential shape recovery is recorded and is shown in Fig. 8. The sample was placed on a heating stage and then heated to 60 °C, in which the sample became soft due to the melting of the crystals of the

soft phase of SMPU. When heated to 100 °C, the sample folded together and was subsequently cooled to room temperature in order to fix its temporary shape (see Fig. 8b). When reheated to 80 °C, the sample started to recover its shape, as seen in Fig. 8c, and a gradual recovery can be seen in Fig. 8d. Finally, the specimen completely recovered its original shape when it was heated to 100 °C. Even though the recovery temperature was higher, sample P3 demonstrated excellent sequential thermal-induced shape recovery process. Additionally, triple-shape memory behaviors were also examined with a thermomechanical analysis using a TA Instruments DMA Q800 system (see supporting information T1). The strain recovery process and its dependence on temperature were recorded for analysis of synthesized composites. Figure 9 presents the strain–time–temperature curves of SMPU–mHOBA composites with various HOBA content. Shape memory cycle tests demonstrate that all synthesized composites exhibit a two-step shape recovery of typical triple-SMEs. On the basis of the DSC and DMA results, the shape memory properties at a higher temperature should be associated with the crystal melting of HOBA, whereas the shape memory properties at low temperature derive from the melting of crystals in the soft phase of SMPU. The shape recovery ratio and shape fixing ratio of SMPU–mHOBA composites in the triple-shape memory cycle are summarized in Table 3. The shape fixing ratio in the first stage is lower than that of the second stage due to the first shape fixing being carried out at a relatively higher temperature while the second shape fixing including both the crystallization of the soft phases of SMPU and HOBA. On the contrary, the shape recovery ratio in the first stage is distinctly higher than that in the second stage. This behavior is observed due to the first shape recovery occurring at a relatively lower temperature, which has a larger recovery force and shows improved strain recovery. In addition, Table 3 also demonstrates that the total shape recovery ratio is smallest in the composites with highest HOBA content, e.g., sample P4. A possible hypothesis for

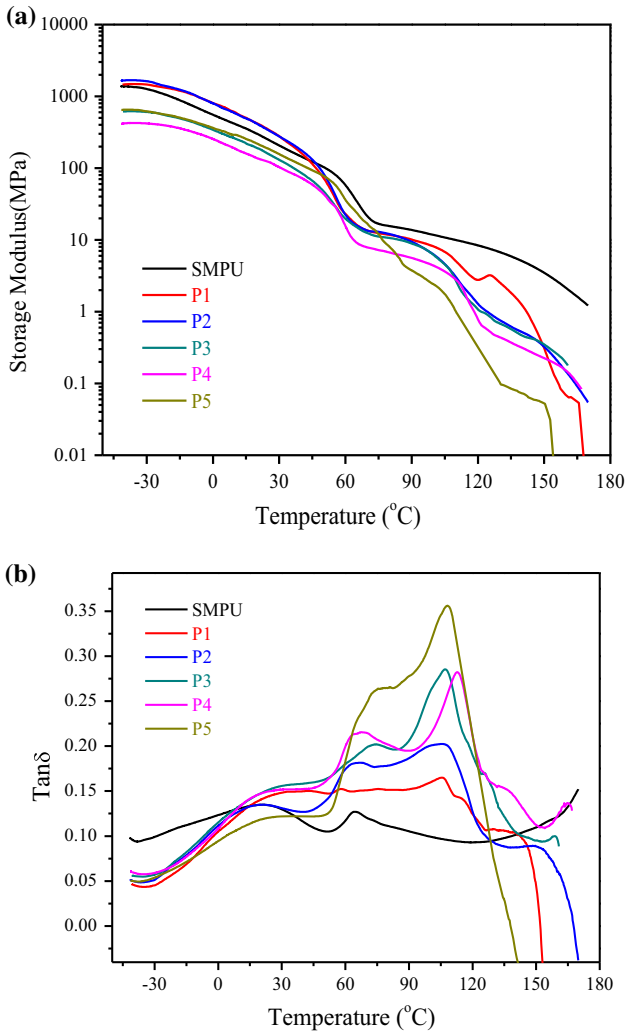


**Figure 7** DMA curves of SMPU–mHOBA composites: **a** storage modulus, **b** tan$\delta$.

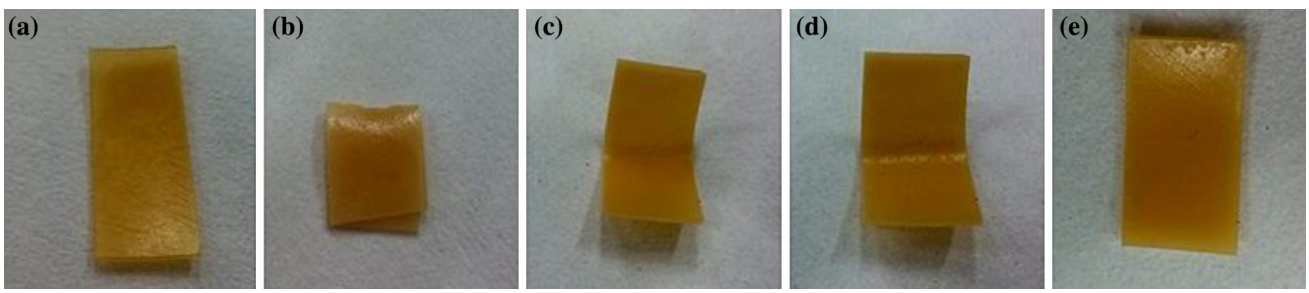


**Figure 8** Sequential shape recovery of sample P3 (**a** original shape, **b** temporary shape after fixing at room temperature, **c** shape recovery at 60 °C, **d** shape recovery at 80 °C, **e** recovered shape at 100 °C).

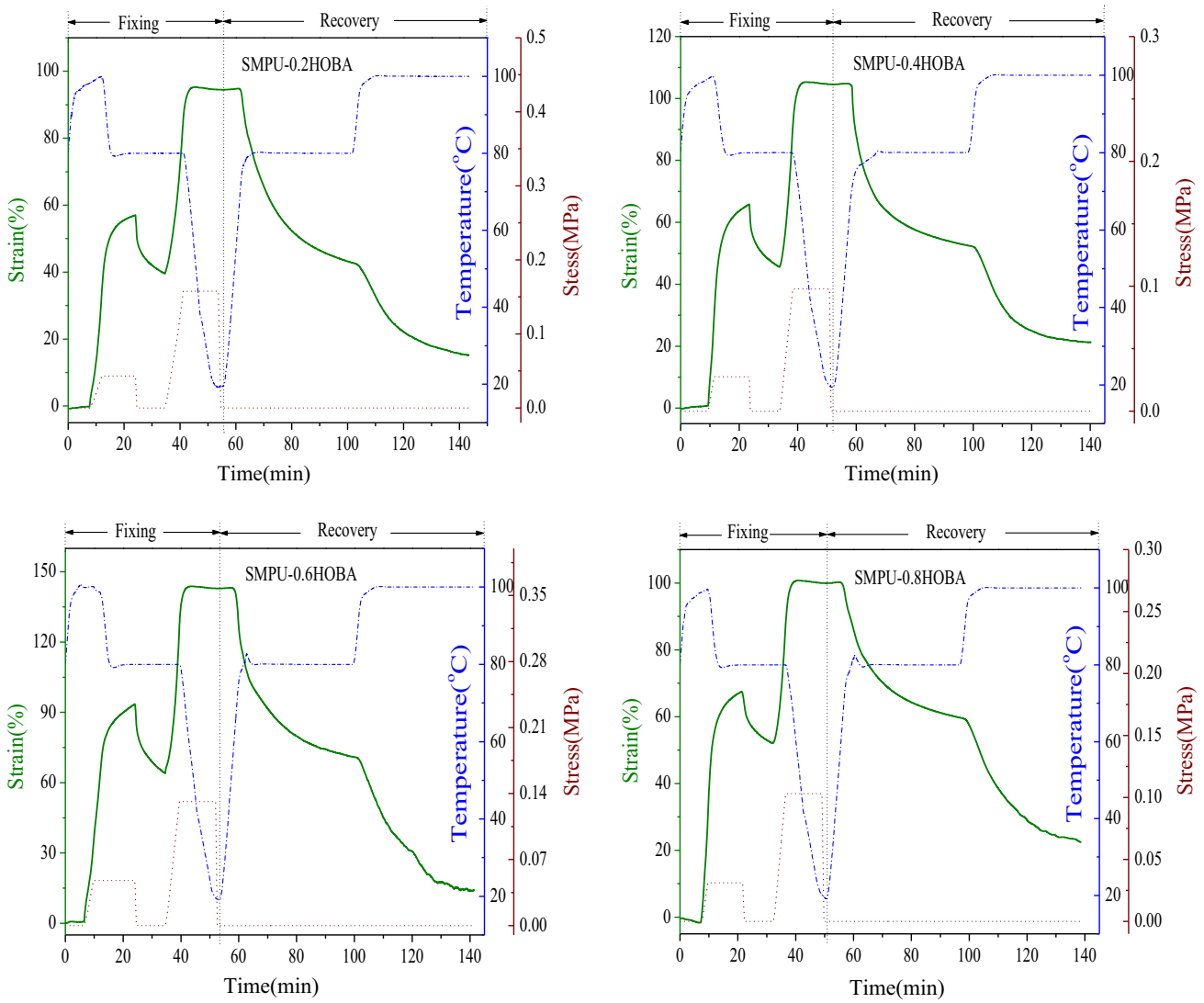


**Figure 9** Triple-shape memory cycles of SMPU–mHOBA composites.

**Table 3** Shape recovery ratio and shape fixing ratio of SMPU–mHOBA composites

| Sample | First shape fixing ratio (%) | Second shape fixing ratio (%) | First shape recovery ratio (%) | Second shape recovery ratio (%) | Total shape recovery ratio (%) |
|---|---|---|---|---|---|
| P1 | 69.61 | 99.36 | 93.60 | 69.66 | 84.18 |
| P2 | 68.53 | 99.16 | 87.73 | 67.13 | 79.48 |
| P3 | 68.90 | 99.33 | 90.67 | 87.40 | 89.80 |
| P4 | 81.33 | 99.81 | 84.02 | 54.15 | 66.97 |

this phenomenon is that HOBA molecules are only physically mixed into polyurethane, while the doped HOBA destroys the physical netpoints serving as a lubricating agent that results in permanent deformation. However, all SMPU–mHOBA composites demonstrate excellent triple-SMEs. Both the strain fixation and strain recovery are programmable. Therefore, the SMPU–mHOBA composites can potentially be implemented in smart optical devices, electronic devices, and sensor-based applications.

## Conclusions

In this paper, SMPU–mHOBA composites were successfully prepared by incorporating HOBA to PEG-based SMPU. The effect of HOBA fillers on the structure and properties was carefully investigated for their shape memory applications. The results demonstrate that the dimerization structure of HOBA is well maintained, which allows for the display of liquid crystalline properties in the bulk composite. The SMPU–HOBA composites form a two-phase separated structure possessing HOBA and SMPU phases, while the doped HOBA content should not exceed 23.92 wt%. Results suggest that the incorporated HOBA promotes crystallization of both the soft and hard segments of SMPU, whereas the crystallization and liquid crystalline behaviors of HOBA are restrained by SMPU. The crystallization mechanism of the hard segment of SMPU is induced by a nucleation mechanism. The heat treatment also influences the morphology and thermal properties of the synthesized composites. The SMPU–HOBA composites show multiple phase transitions with a significant multi-step modulus change. Therefore, the SMPU–mHOBA composites exhibit excellent triple-SMEs in which the strain recovery is activated by the melting of crystals in the soft phase of SMPU and HOBA.

## Acknowledgements

This work was supported by the National Natural Science Foundation of China (Grant Nos. 61425007, 61377090, and 61575128), the Natural Science Foundation of Guangdong (Grant Nos. 2014A030313559, 2016A030313050), the Special Research Foundation of Shenzhen Overseas High-level Talents for Innovation and Entrepreneurship (Grant No. KQCX201208 07153115869), the Nanshan District Key Lab for Biopolymers and Safety Evaluation (No. KC2014Z DZJ0001A), the Science and Technology Project of Shenzhen City (Grant Nos. JCYJ20140828163633993, ZDSYS201507141105130, CYZZ20150827160341635).

**Electronic supplementary material:** The online version of this article (doi:10.1007/s10853-016-0554-8) contains supplementary material, which is available to authorized users.

## References

[1] Zhao Q, Qi HJ, Xie T (2015) Recent progress in shape memory polymer: new behavior, enabling materials, and mechanistic understanding. Prog Polym Sci 49–50:79–120

[2] Hager MD, Bode S, Weber C, Schubert US (2015) Shape memory polymers: past, present and future developments. Prog Polym Sci 49–50:3–33

[3] Liu YJ, Du HY, Liu LW, Leng JS (2014) Shape memory polymers and their composites in aerospace applications: a review. Smart Mater Struct 23(2):023001

[4] Meng H, Li G (2013) A review of stimuli-responsive shape memory polymer composites. Polymer 54:2199–2221

[5] Kumar KSS, Biju R, Nair CPR (2013) Progress in shape memory epoxy resins. React Funct Polym 73:421–430

[6] Sun L, Huang WM, Ding Z, Zhao Y, Wang CC, Purnawali H, Tang C (2012) Stimulus-responsive shape memory materials: a review. Mater Des 33:577–640

[7] Lu HB, Lu CR, Huang WM, Leng JS (2015) Chemo-responsive shape memory effect in shape memory polyurethane triggered by inductive release of mechanical energy storage undergoing copper (II) chloride migration. Smart Mater Struct 24(7):035018–035018

[8] Singhal P, Small W, Cosgriff-Hernandez E, Maitland DJ, Wilson TS (2014) Low density biodegradable shape memory polyurethane foams for embolic biomedical applications. Acta Biomat 10:67–76

[9] Ronda JC, Del Rio E, Lligadas G, Galia M, Cadiz V, Meier M (2011) Shape memory polyurethanes from renewable polyols obtained by ATMET polymerization of glyceryl triundec-10-enoate and 10-undecenol. Macromol Chem Phy 212:1392–1399

[10] Ji FL, Hu JL, Han JP (2011) Shape memory polyurethane-ureas based on isophorone diisocyanate. High Perform Polym 23:177–187

[11] Zhang YM, Wang C, Pei XQ, Wang QH, Wang TM (2010) Shape memory polyurethanes containing azo exhibiting photoisomerization function. J Mater Chem 20:9976–9981

[12] Zhang DW, Liu YJ, Leng JS (2010) Magnetic field activation of thermoresponsive shape-memory polymer with embedded micron sized Ni powder. Adv Mater Res 123–125:995–998

[13] Zhang DW, Leng JS, Liu YJ (2008) Influence of radialization dosage on shape memory effect of polystyrene copolymer. Adv Mater Res 47–50:690–693

[14] Li L, Li Y, Li JS, Yao L, Mak A, Ko F, Qin L (2008) Antibacterial and nontoxic nano silver PLLA composites for tissue engineering. Adv Mater Res 47–50:849–852

[15] Lan X, Leng JS, Liu YJ, Du SY (2008) Investigate of electrical conductivity of shape-memory polymer filled with carbon black. Adv Mater Res 47–50:714–717

[16] Golbang A, Kokabi M (2010) Magnetic Field Actuation of shape Memory Nanocomposites. Adv Mater Res 123–125:999–1002

[17] Sun L, Huang WM, Wang CC, Ding Z, Zhao Y, Tang C, Gao XY (2014) Polymeric shape memory materials and actuators. Liq Cryst 41:277–289

[18] Kasi RM, Ahn SK, Deshmukh P, Gopinadhan M, Osuji CO (2011) Side-chain liquid crystalline polymer networks: exploiting nanoscale smectic polymorphism to design shape-memory polymers. ACS Nano 5:3085–3095

[19] Hiraoka K, Tashiro T, Kobayashi M, Kazama R, Sagano W (2010) Symmetry and stimulus response of chiral smectic liquid-crystalline elastomers. In: Khoo IC (ed) Proceedings of SPIE, liquid crystals XIV, California, 1–2 and 4 August 2010

[20] Finkelmann H, Happ M, Portugal M, Ringsdorf H (1978) Liquid-crystalline polymers with biphenyl-moieties as mesogenic group. Macromol Chem Phy 179:2541–2544

[21] Sonin AS, Churochkina NA, Kaznacheev AV (2008) Polymer liquid crystalline composite for optical irradiation control. Polym Sci Ser B 50:30–34

[22] Ahir SV, Tajbakhsh AR, Terentjev EM (2006) Self-assembled shape-memory fibers of triblock liquid-crystal polymers. Adv Funct Mater 16:556–560

[23] Chen SJ, Yuan HM, Zhuo HT, Chen SG, Yang HP, Ge ZC, Liu JH (2014) Development of liquid-crystalline shape-memory polyurethane composites based on polyurethane with semi-crystalline reversible phase and hexadecyloxybenzoic acid for self-healing applications. J Mater Chem C 2:4203–4212

[24] Chen SJ, Yuan HM, Ge ZC, Chen SG, Zhuo HT, Liu JH (2014) Insights into liquid-crystalline shape-memory polyurethane composites based on an amorphous reversible phase and hexadecyloxybenzoic acid. J Mater Chem C 2:1041–1049

[25] Chen SJ, Yuan HM, Chen SG, Yang HP, Ge ZC, Zhuo HT, Liu JH (2014) Development of supramolecular liquid-crystalline polyurethane complexes exhibiting triple-shape functionality using a one-step programming process. J Mater Chem A 2:10169–10181

[26] Chen SJ, Mo FN, Chen SG, Ge ZC, Yang HP, Zuo JD, Liu XK, Zhuo HT (2015) New insights into multi-shape memory behaviours and liquid crystalline properties of supramolecular polyurethane complexes based on pyridine-containing polyurethane and 4-octyldecyloxybenzoic acid. J Mater Chem A 3:19525–19538

[27] Ban J, Zhu L, Chen SJ, Wang YP (2016) The impact of liquid crystal fillers on structure and properties of liquid-crystalline shape-memory polyurethane composites I: 4-dodecyloxybenzoic acid. J Mater Sci 51:10229–10244. doi:10.1007/s10853-016-0251-7

[28] Mo FN, Zhou FX, Chen SJ, Yang HP, Ge ZC, Chen SG (2015) Development of shape memory polyurethane based on polyethylene glycol and liquefied 4,4 '-diphenylmethane diisocyanate using a bulk method for biomedical applications. Polym Int 64:477–485

[29] Nosikova LA, Kudryashova ZA, Iskhakova LD, Tsivadze AY (2007) Solid-phase polymorphism of *p-n*-hexyloxy- and *p-n*-heptyloxybenzoic acids. Russ J Phys Chem A 81:1263–1266

[30] Shatalova AM, Kresse H, Shandryuk GA, Bondarenko GN, Kuptsov SA, Talroze RV (2004) The role of the alien proton acceptor on the formation of LC structure in H-bonded monomeric and polymeric derivatives of alkoxybenzoic acids. J Mol Struct 708:7–14

[31] Chen H, Liu Y, Gong T, Wang L, Zhao K, Zhou S (2013) Use of intermolecular hydrogen bonding to synthesize triple-shape memory supermolecular composites. RSC Adv 3:7048–7056

[32] Zhu Y, Hu J, Choi K-F, Meng Q, Chen S, Yeung K-W (2008) Shape memory effect and reversible phase crystallization process in SMPU ionomer. Polym Adv Technol 19:328–333